

Ocean heat transport into the Arctic in the twentieth and twenty-first century in EC-Earth

Torben Koenigk · Laurent Brodeau

Received: 1 February 2013 / Accepted: 28 May 2013 / Published online: 7 June 2013
© The Author(s) 2013. This article is published with open access at Springerlink.com

Abstract The ocean heat transport into the Arctic and the heat budget of the Barents Sea are analyzed in an ensemble of historical and future climate simulations performed with the global coupled climate model EC-Earth. The zonally integrated northward heat flux in the ocean at 70°N is strongly enhanced and compensates for a reduction of its atmospheric counterpart in the twenty first century. Although an increase in the northward heat transport occurs through all of Fram Strait, Canadian Archipelago, Bering Strait and Barents Sea Opening, it is the latter which dominates the increase in ocean heat transport into the Arctic. Increased temperature of the northward transported Atlantic water masses are the main reason for the enhancement of the ocean heat transport. The natural variability in the heat transport into the Barents Sea is caused to the same extent by variations in temperature and volume transport. Large ocean heat transports lead to reduced ice and higher atmospheric temperature in the Barents Sea area and are related to the positive phase of the North Atlantic Oscillation. The net ocean heat transport into the Barents Sea grows until about year 2050. Thereafter, both heat and volume fluxes out of the Barents Sea through the section between Franz Josef Land and Novaya Zemlya are strongly enhanced and compensate for all further increase in the inflow through the Barents Sea Opening. Most of the heat transported by the ocean into the Barents Sea is passed to the atmosphere and contributes to warming of the

atmosphere and Arctic temperature amplification. Latent and sensible heat fluxes are enhanced. Net surface long-wave and solar radiation are enhanced upward and downward, respectively and are almost compensating each other. We find that the changes in the surface heat fluxes are mainly caused by the vanishing sea ice in the twenty first century. The increasing ocean heat transport leads to enhanced bottom ice melt and to an extension of the area with bottom ice melt further northward. However, no indication for a substantial impact of the increased heat transport on ice melt in the Central Arctic is found. Most of the heat that is not passed to the atmosphere in the Barents Sea is stored in the Arctic intermediate layer of Atlantic water, which is increasingly pronounced in the twenty first century.

Keywords Arctic · Ocean heat transport · Ocean volume transport · Climate change · Climate variability · Global coupled modelling

1 Introduction

Observations of the last decades show an ongoing climate change in the Arctic regions. The observed warming in the Arctic is about twice or more the rate of the global mean warming in the last decades (ACIA 2005; IPCC 2007, Richter-Menge and Jeffries 2011). The warming in the Arctic is concurrent with a large reduction of sea ice cover (Comiso et al. 2008; Stroeve et al. 2012) with a new September ice extent minimum in 2012.

Besides the ice-albedo feedback (Serreze et al. 2009), enhanced meridional energy transport (Graversen et al. 2008), changes in clouds and water vapour (Graversen and Wang 2009, Liu et al. 2008), enhanced ocean heat transport

T. Koenigk (✉)
Rosby Centre, Swedish Meteorological and Hydrological
Institute, 60176 Norrköping, Sweden
e-mail: torben.koenigk@smhi.se

L. Brodeau
Department of Meteorology, Bert Bolin Centre for Climate
Research, Stockholm University, 10691 Stockholm, Sweden

into the Arctic is a likely source for Arctic temperature amplification (Spielhagen et al. 2011). However, changes in the ocean transports are more difficult to detect due to large variations on long time scales and sparse observations in space and time. Polyakov et al. (2004) showed that the Atlantic water masses in the Arctic are dominated by low frequency variations at timescales of 50–80 years. They also showed a close connection of these variations with sea ice and atmospheric. Analyses by Dickson et al. (2000) indicated a close relation of interannual to decadal variations of ocean heat and volume fluxes to large scale atmospheric patterns like the North Atlantic Oscillation/Arctic Oscillation (NAO/AO). However, more recent studies by Goosse and Holland (2005) and Semenov (2008) showed that the relation between NAO and ocean fluxes vary with time.

Variations of the inflowing Atlantic water into the Barents Sea affect Arctic climate variability (Furevik 2001; Sandø et al. 2010). Semenov et al. (2009) and Bengtsson et al. (2004) argued that enhanced ocean heat transport into the Barents Sea leads to reduced ice, enhanced oceanic heat release and locally reduced pressure. This feeds positively back on the oceanic heat inflow and can result in dramatic changes in the Barents Sea region and contributes to amplified climate change in the Arctic. A number of other studies showed a similar positive feedback in the Barents Sea (Ådlandsvik and Loeng 1991; Ikeda 1990; Goosse et al. 2003; Goosse and Holland 2005). Results from a regional Arctic Ocean model study by Karcher et al. (2003) suggested that the inflow of Atlantic warm water into the Arctic is no steady process but occurs in the form of events and is triggered both by temperature anomalies and velocity anomalies of the inflowing water.

Observations (e.g. Skagseth et al. 2008, Dmitrenko et al. 2008) indicate an increase in the ocean heat transport into the Arctic through Barents Sea. Årthun et al. (2012) and Schlichtholz (2011) related this increase to the recent sea ice reduction in the Barents Sea. Most of the inflowing ocean heat through the Barents Sea Opening is given to the atmosphere in the Barents Sea (Årthun and Schrum 2010; Smedsrud et al. 2010), here the heat flux can reach up to 500 W/m^2 (Häkkinen and Cavalieri 1989). The warm surface waters are cooled down, become heavy and form the relatively warm intermediate layer in the Arctic Ocean. These warm Atlantic waters are separated from the surface by a cold and fresh surface layer in the Arctic and have no contact to the surface in the interior of the Arctic (Aagaard et al. 1981; Rudels et al. 1996). Changes in the water mass constitutions might have severe consequences for the entire Arctic climate system.

Woodgate et al. (2006) analyzed ocean heat, volume and freshwater transports through the Bering Strait between 1990 and 2005. They showed high interannual variability

with the largest heat transports at the end of the time series due to both warmer waters and larger volume flux. Since the inflowing water has rather low density an increase in heat transport through the Bering Strait might have severe consequences for sea ice melt. Shimada et al. (2006) found that increased temperatures of the Arctic Pacific surface waters in the late 90 s were followed by a marked decrease in sea ice in the Pacific Arctic sector.

In a recent article, Vavrus et al. (2012) showed a strong warming of the Arctic Ocean, with a maximum of 2.5 K at about 400 m, until the end of the twenty first century in RCP8.5 scenario simulations with CCSM4. They identified the warming of the inflowing Atlantic water through Barents Sea as the main reason for the warming of the intermediate layer. Koenigk et al. (2013) (hereafter referred to as KEA13) found the largest sea ice and atmospheric temperature changes of the Arctic in the Barents Sea together with strongly enhanced ocean heat transport into the Barents Sea in future scenario simulations with EC-Earth.

This study analyzes variability and trends of the ocean heat transports into the Arctic in detail in both historical and future scenario simulations with EC-Earth. Particularly, we seek to investigate the role of the ocean heat transport into the Barents Sea for the large sea ice reduction and atmospheric changes found in EC-Earth by KEA13.

The study is organized as follows. After this introduction, the model and the simulations are described. Section 3 presents the results from the model simulations, starting with the large-scale northward heat transports followed by more detailed analyses of the ocean volume and heat transports through the Arctic Straits and the analysis of the heat budget of the Barents Sea. Section 4 provides a summary and conclusions from this study.

2 Model and simulations

2.1 Model description

The model used in this study is the global coupled climate model EC-Earth (Hazeleger et al. 2010). The Integrated Forecast System (IFS) of the European Centre for Medium Range Weather Forecasts (ECMWF) constitutes the atmosphere component and the Nucleus for European Modelling of the Ocean (NEMO), developed by the Institute Pierre Simon Laplace (IPSL), the ocean component (Madec 2008). Here, we used the model version 2.3, which has been used for all Coupled Model Intercomparison Project phase 5 (CMIP5)-simulations with EC-Earth.

The atmosphere component is used at a T159 spectral resolution with 62 vertical levels. It is based on cycle 31r1 of IFS, but includes some improvements from later cycles.

The most important improvements are the convection scheme by Bechtold et al. (2008), the land surface scheme H-TESSEL (Balsamo et al. 2009), and a new snow scheme (Dutra et al. 2010).

NEMO, the ocean component, uses the so-called ORCA1 horizontal grid configuration which has a resolution of about 1 degree (with a refinement of the grid at the equator) and runs on 42 vertical levels. ORCA is a family of tri-polar grids with poles located over northern North America, Siberia and Antarctica. The version used in EC-Earth v2.3 is based on NEMO version 2.0 and includes the Louvain la Neuve sea-ice model version 2 (LIM2, Fichefet and Morales Maqueda 1997, Bouillon et al. 2009), which is a dynamic-thermodynamic sea-ice model.

The atmosphere and ocean/sea ice parts are coupled through the OASIS (Ocean, Atmosphere, Sea Ice, Soil) coupler (Valcke 2006).

The climate of the model in present-day and pre-industrial control simulations is described in more details by Sterl et al. (2012) and Hazeleger et al. (2012). An overview of Arctic climate of the twentieth and twenty first century as simulated by EC-Earth is presented by KEA13.

2.2 Scenario simulations

An ensemble of historical simulations (1850–2005) and future simulations (2006–2100) based on forcing schemes suggested by the CMIP5 was performed with EC-Earth. An ensemble of three historical twentieth century simulations was obtained by initializing from different times of a long pre-industrial simulation with EC-Earth. Each of these historical simulations was continued with two different twenty first century simulations, based on the Representative Concentration Pathways (RCP) 4.5 and 8.5 emission scenarios. One RCP2.6 simulation was also performed starting from one of the three historical simulations. These are the same simulation as used in KEA13.

In the following sections, ensemble means are used if nothing else is stated. Note that only one RCP2.6 scenario simulation was performed.

Furthermore, we often use detrended data to calculate correlations between variables and analyse the natural variability of the system. Hereby, the problem arises that the trend changes with time in the period 1850–2100. On the other hand, natural variations in heat and volume fluxes are subject to multi-decadal variations. Thus, subtracting running mean trends of shorter time periods might lead to uncertainties as well. Most heat and volume fluxes in EC-Earth show two periods with obvious differences in trends: 1850–1950 and 1950–2100. 1850–1950 shows more or less constant fluxes while after 1950 substantial trends occur. We calculated thus linear trends separately for the periods 1850–1950 and 1950–2100. In Sect. 3.2, we compare

correlations in the historical period with those of the period 2050–2099. Here, we calculate trends for the periods 1850–1950, 1950–2005 and 2050–2099 separately and subtract the trends from the original time series.

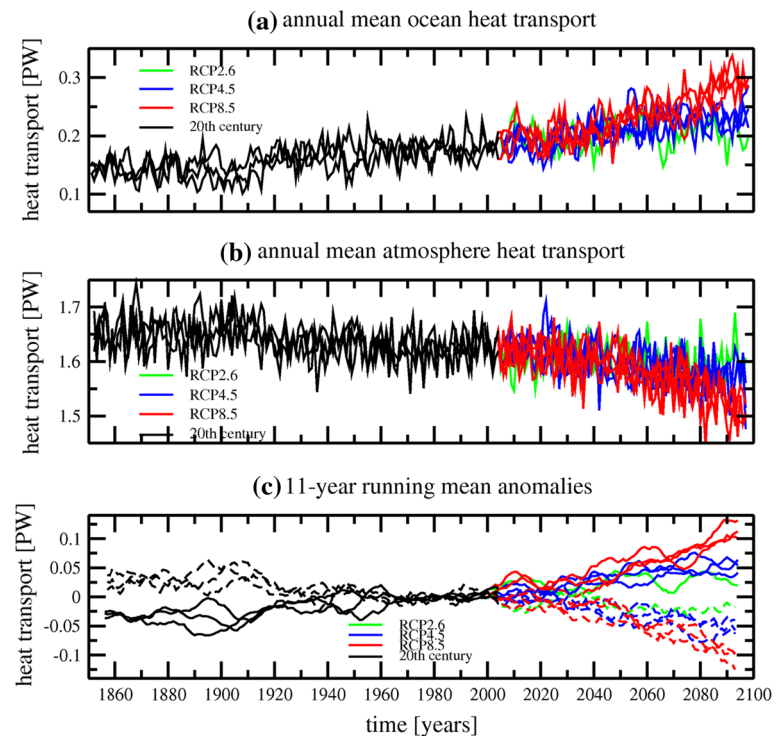
3 Results

3.1 Heat transport into the Arctic

The total heat transport into the Arctic (atmosphere + ocean heat transport) is dominated by the atmospheric transport (Fig. 1). The atmospheric heat flux to the north across 70°N has been calculated as residuum of the integrated (over 70–90°N) net top of the atmosphere radiation and net surface heat fluxes. When it comes to the ocean, we used two different approaches to calculate the northward ocean heat transport: First, it is calculated as residuum of the integrated surface fluxes and the change in ocean heat content north of 70°N. Second, we estimate it by calculating the product of velocity across 70°N, the difference of ocean temperature to a reference temperature (Tref), the density of the water mass and the specific heat capacity of the water. Similar to most other studies, we use 0 °C as reference temperature. In the following, we will use the second method. However, the results from both methods give a similar value for the northward transport across 70°N of about 0.17PW and annually averaged values are correlated with 0.95. The ocean heat transport across 70°N is almost totally dominated by the heat transport in the Atlantic in EC-Earth. Observational based estimates by Oliver and Heywood (2003) showed a transport of 0.2 ± 0.08 PW across a section at approximately 70°N between Greenland and Norway.

The atmospheric heat transport across 70°N in EC-Earth is almost 10 times larger than the ocean heat transport and reaches about 1.6PW at the end of the twentieth century. However, the standard deviation of annually averaged values is <2 times larger for the atmospheric transport than the oceanic transport; decadal variations of the heat fluxes are of the same size. The decadal anomalies are often canceling out each other. This feature is known as Bjerknes compensation (Bjerknes 1964) and has recently been analyzed in modeling studies by van der Swaluw et al. (2007) and Jungclaus and Koenigk (2010). Van der Swaluw et al. (2007) defined a compensate rate (CR) in percentage of the maximum local total northward transport. The CR is 31 % in our twentieth century simulations at 70°N, which compares to a CR of 55 % at 70°N in HADCM3 (Van der Swaluw et al. 2007) and 33 % in ECHAM5/MPIOM (Jungclaus and Koenigk, 2010). The correlation coefficient between 10-year running means of detrended ocean and atmospheric heat transports reaches -0.72 in EC-Earth,

Fig. 1 **a** Annual mean ocean heat transport across 70°N in PW in the twentieth century simulations (black), RCP2.6 (green), RCP4.5 (blue) and RCP8.5 (red) simulations. **b** Annual mean atmosphere heat transport across 70°N in the twentieth and twenty first century simulations. **c** 11-year running mean anomalies of ocean (solid) and atmosphere (dashed) heat transport across 70°N. Reference period is 1980–1999



while it is -0.62 and -0.8 in ECHAM5/MPIOM and HADCM3, respectively. We found the highest correlation when the ocean heat transport leads the atmospheric heat transport by about 2 years.

The correlation between decadal variations in the ocean heat flux across 70°N and the Arctic air temperature at 2 m height (T2m), averaged over 70–90°N reaches 0.62 when the heat transport leads by 3 years. The highest correlation between atmospheric heat transport and Arctic T2m is 0.65 at a lag of 1 year.

In the twenty first century, the atmospheric heat transport to the north is reduced. This reduction is compensated by an increase in the ocean heat transport, which reaches about 0.3PW in the RCP8.5 at the end of the twenty first century. Decadal anomalies of the ocean heat transport are large also in the twenty first century and the three realizations based on the same emission scenario deviate a lot from each other. The CR in the twenty first century remains almost unchanged ($CR = 0.29$ for RCP4.5 and 0.32 for RCP8.5 for detrended decadal means averaged over 2050–2099) indicating that the Bjerknes compensation is not substantially changing in our model.

3.2 Volume and heat transports through Arctic Straits

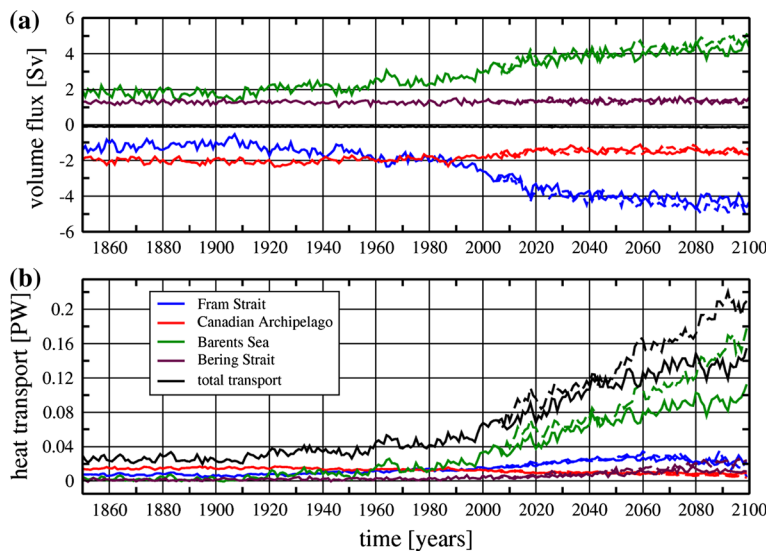
This section discusses changes and variations of the volume and heat fluxes through the Arctic Straits more in detail. We used the following sections as openings for the Arctic Ocean: Barents Sea Opening (here we used a section

between Svalbard and the Kanin Peninsula at about 68.5°N and 45°E as done in KEA13), Fram Strait (at about 80°N), Canadian Archipelago (Lancaster Sound and Smith Sound) and Bering Strait (at 66°N). Thereby, we used hydrographic sections which are either zonal or meridional on the ocean model grid and calculated the volume flux as spatial integral of the normal component of the velocity across the section and the heat flux as product of velocity and heat capacity of the water as described before. Again, we use 0 °C as reference temperature. The mean heat fluxes depend on T_{ref} but changes in the fluxes and heat budgets are insensitive to changes in T_{ref} .

In all our simulations, regardless of the future scenario, the volume flux through the Bering Strait is relatively constant and corresponds roughly to an input of about 1.4 Sv into the Arctic Ocean (Fig. 2a). We find a net outflow through Fram Strait of about 2.3 Sv and a net inflow through the Barents Sea Opening of roughly 2.7 Sv in the period 1980–2000. The outflow through the Canadian Archipelago sums up to 1.9 Sv in our model. These values compare relatively well to observational estimates of about 2 Sv through the Barents Sea Opening (Skagseth 2008), -2 Sv through Fram Strait (Schauer et al. 2008), -1.3 Sv through the Canadian Archipelago (-0.7 through Lancaster Sound (Melling et al. 2008) and -0.57 through Nares Strait (Münchow and Melling 2008)) and 0.8 Sv through Bering Strait (Woodgate and Aagaard 2005).

In the twenty first century, the Arctic Ocean tends to import less water northward through the Greenland-

Fig. 2 **a** Annual mean ocean volume fluxes in Sv through Fram Strait (blue), Canadian Archipelago (red), Barents Sea (green) and Bering Strait (maroon) and the sum of all (black) in RCP4.5 (solid) and RCP8.5 (dashed) simulations. Ensemble means are shown. Volume fluxes into the Arctic are positive. **b** The same as (a) but for ocean heat transports (based on Figure 18b, Koenigk et al. 2013)



Norway section (not shown) and—since Bering Strait flow remains roughly constant—tends to export less water southward through the Canadian Archipelago. However, significantly more water flows northward through the Barents Sea Opening, which is overcompensated by more water leaving southward through the Fram Strait. The sum of all fluxes is negative with about -0.1 Sv, which is balanced by river runoff and a positive P-E balance over the Arctic Ocean (KEA13). In the RCP8.5 scenario simulations, the changes in the flows through the Barents Sea Opening and the Fram Strait are slightly more amplified than in the RCP4.5 simulations.

The total heat transport into the Arctic Ocean sums up to about 50TW (20TW into the Barents Sea and 15TW each through Fram Strait and Canadian Archipelago) at the end of the twentieth century (Fig. 2b). The ocean heat transport through Fram Strait seems to be somewhat underestimated compared to observations of 30–40TW by Schauer et al. (2008) while the transport into Barents Sea is relatively well simulated. In addition to our Barents Sea Opening connecting Svalbard with the Kanin Peninsula we calculated also the heat flux across a line connecting Svalbard and northern Norway for better comparison with observational results. The heat flux across this line reaches about 50TW and is thus 30TW larger than across the line Svalbard-Kanin Peninsula. However, the correlation between the two heat fluxes is nearly one and the offset of 30TW remains almost constant throughout the entire twenty first century. The range of the estimated heat transport into the Barents Sea based on observations is large and varies between around 30 and 160TW (Hopkins 1991; Simonsen and Haugan 1996). Recent estimates by Skagseth (2008) indicate a heat transport of about 50TW and high resolution model results by Aksenov et al. (2010) 60TW. However, comparison to observations is difficult since observational

time series are short and not exactly at the same sections as in our model study.

In the twenty first century, the total heat inflow into the Arctic is strongly increased, mainly due to increased heat transport into the Barents Sea (Fig. 2b). The differences between RCP4.5 and RCP8.5 simulations are much larger for the heat flux than for the volume flux into the Barents Sea, indicating that mainly temperature increase is responsible for these differences.

In this study, we extend the results from KEA13 by investigating the variability and trends of the simulated heat fluxes. For this purpose we divided the heat fluxes into anomalies related to temperature anomalies ($T'V$), volume flux anomalies ($V'T$), and the product of temperature and volume flux anomalies ($T'V'$, Fig. 3). The anomalies are calculated in reference to the mean of the time period 1980–1999 (T , V).

The heat transport through Barents Sea grows substantially already in the twentieth century. The increase of heat transport is mainly due to a warming of the inflowing water ($T'V$) into the Barents Sea. However, also increasing volume flux (as also seen in Fig. 2a) contributes to a smaller part ($V'T$). $T'V$ and $V'T$ are positively correlated and consequently, $T'V'$ is positive before the reference period and gradually reduced during the twentieth century. The interannual variations of the three components are of similar size in the twentieth century.

In the twenty first century, a strong increase in both $T'V$ and $T'V'$ can be seen. The increase in $V'T$ is comparatively small. The warming of the inflowing water governs the large increase in the ocean heat transport into the Barents Sea in the twenty first century but still, the components are highly positively correlated to each other. The stronger the emission scenario the larger the heat fluxes. Similar to our results, measurements of the heat flux

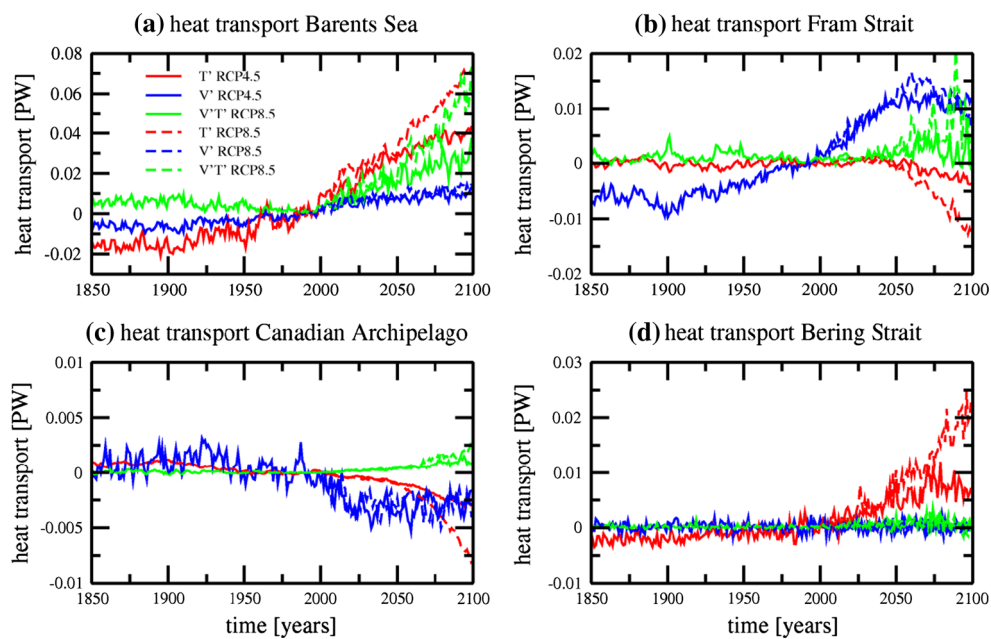


Fig. 3 **a** Annual mean ocean heat transport anomalies in PW through Barents Sea due to temperature anomalies ($T'V'$), volume flux anomalies ($V'T$) and the product of volume and temperature anomalies ($V'T'$). The reference period is 1980–1999. Shown are

ensemble means of RCP4.5 (*solid*) and RCP8.5 (*dashed*) simulations. **b** The same as **(a)** for the Fram Strait. **c** The same as **(a)** for the Canadian Archipelago. **d** The same **(a)** for the Bering Strait

variations in the Norwegian Atlantic Current by Orvik and Skagseth (2005) indicate that the observed trend in their time series is dominated by temperature anomalies. However, while our model results indicate that volume flux and temperature anomalies are to the same extent responsible for interannual variations of the ocean heat transport, they found variations in the volume flux as main reason.

The trend and the variability of the heat transport through Fram Strait are mainly governed by volume flux changes ($V'T$) in the twentieth century. Volume flux anomalies lead to a substantial increase in the heat transport until about 2050, thereafter the increase is leveled out or even slightly decreased (see Fig. 3b). The impact of temperature variations are small until the middle of the twenty first century but are contributing to decreasing heat transports thereafter. This is mainly caused by a warming of the southward, outflowing, surface near water masses. As long as temperature is below T_{ref} , the outflowing water is contributing to heat inflow into the Arctic Ocean. This changes as soon as the water temperature increases and exceeds T_{ref} .

The variations of $T'V'$ become large at the end of the twenty first century due to large anomalies in both T and V compared to the period 1980–1999.

Variations of the heat transport through the Canadian Archipelago are mainly governed by the volume flux through the archipelago. The temperature is below $0\text{ }^{\circ}\text{C}$, which means that the outflowing water constitutes a source

of heat for the Arctic Ocean. Temperature variations are small and play a minor role in the twentieth century. In the twenty first century, temperature increases and comes close to T_{ref} , so that the outflowing water is not any longer a large source of heat for the Arctic. Also the volume flux out of the Arctic through the Canadian Archipelago is reduced. Consequently, the northward ocean heat transport through the Canadian Archipelago is reduced in the twenty first century. The transport variations are still dominated by variations of the volume flux.

The behavior of the heat transport through Bering Strait resembles that into Barents Sea: in the twentieth century, variations in velocity and temperature contribute equally to the total heat transport variations while in the twenty first century, it is mainly the temperature increase that leads to enhanced total heat transport through Bering Strait. However, the increase is small compared to the increase of heat transport into the Barents Sea.

In the following, we concentrate our analysis on the ocean heat transport into the Barents Sea since it shows by far the largest signal in future (Fig. 2b) and has the potential to strongly affect Arctic climate change. Figure 4 shows the correlation patterns of the Barents Sea heat transport components with sea level pressure (SLP), 2 m air temperature (T_{2m}) and sea ice thickness. A reduction of SLP over the Iceland–Greenland area and an increase over parts of Europe and the North Atlantic together with a strong SLP gradient across the Barents Sea Opening are

connected to positive anomalies in the total heat transport, in $V'T$ and $T'V$. This pattern is connected to enhanced south-westerly winds in the Nordic Seas and increases the volume flux into the Barents Sea, which fits well to observations by Skagseth et al. (2008) and model results by Goosse and Holland (2005). At the same time, warmer than normal water masses are transported northward into the Barents Sea. Obviously, the same atmospheric circulation pattern is leading to increased temperature and increased velocity of the water masses. This explains why the total Barents Sea heat transport, $V'T$ and $T'V$ are all highly correlated with each other. However, the correlation pattern is slightly more pronounced for $V'T$ at lag 0 than for $T'V$. This is opposite when SLP leads by 1 year: the correlation is still high for $T'V$ but strongly reduced for $V'T$. The reason is that the velocity of the water masses, particularly at the surface, is rapidly responding to increased south westerly winds, while it takes longer until warm water masses are advected from south towards the Barents Sea Opening.

Our model results agree with results by Dickson et al. (2000) who showed that a positive NAO pattern increases both velocity and temperature of the Atlantic water entering Barents Sea. Also results by Sandø et al. (2010)

indicate that the variability in the Barents Sea heat inflow is strongly linked to the NAO.

The corresponding correlations between ocean heat transports and air temperature show warm anomalies in the Barents Sea and surroundings. The correlation pattern between heat transport and T2m looks very similar for the total heat transport into Barents Sea, $T'V$ and $V'T$. Also the correlation of the heat transport with sea ice thickness shows high negative values in the Barents Sea.

It is difficult to estimate from our simulations how much of this warming and ice reduction is due to the forcing wind pattern and what part is due to enhanced ocean heat transport. Studies by Sorteberg and Kvingedal (2006) and Koenigk et al. (2009) analyzed sea ice anomalies in the Barents Sea and showed that they are mainly governed by the atmospheric circulation. Regional model results by Årthun et al. (2012) indicate instead a strong contribution of the ocean heat transport at interannual time scales. Koenigk et al. (2009) found also that the temperature response to isolated ice anomalies in the Barents Sea is mainly concentrated to the Barents and Kara Seas region and does not extend as far southward as in our lag-0 correlation pattern.

Correlations of 11-year running mean values show generally slightly higher correlations but similar spatial

Fig. 4 **a** Correlation between detrended annual mean heat transport into the Barents Sea and SLP in the historical simulations, 1850–2005. **b** Correlation between detrended heat transport anomalies due to temperature anomalies (T') and SLP. **c** Correlation between detrended heat transport anomalies due to volume flux anomalies (V') and SLP. **d, e, f** The same as (a, b, c) but for T2m. **g, h, i** The same as (a, b, c) but for sea ice thickness

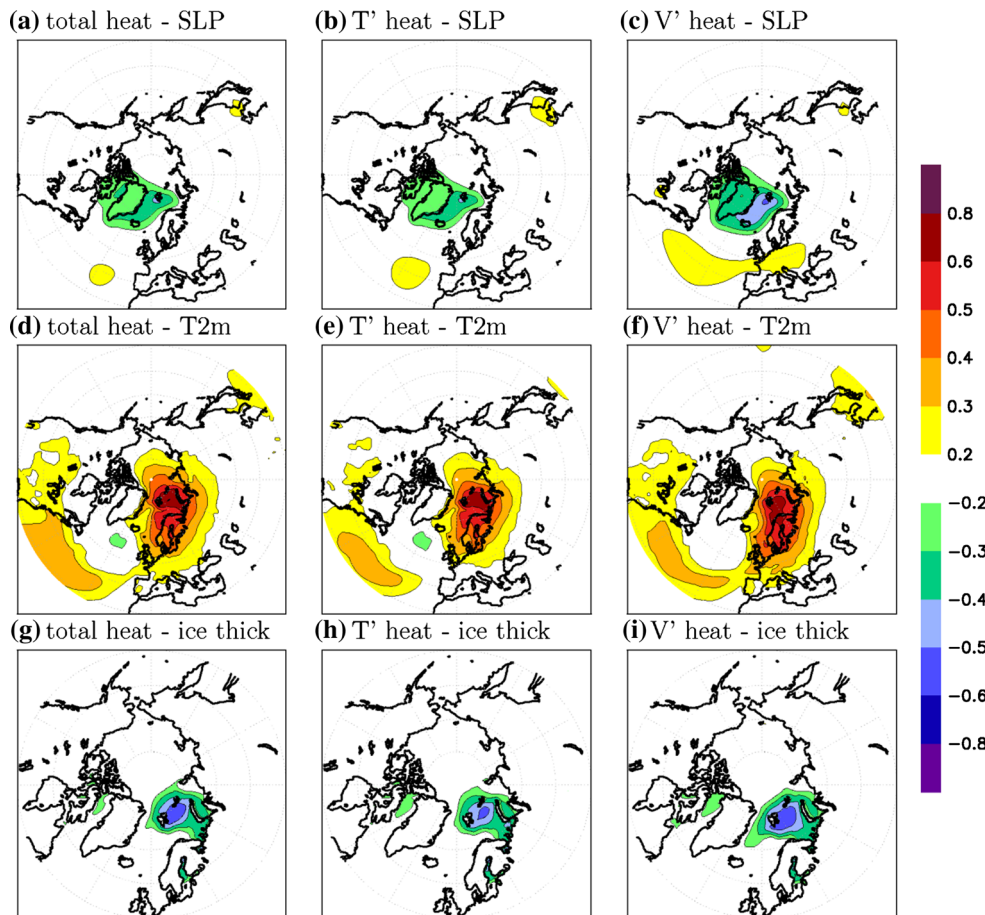
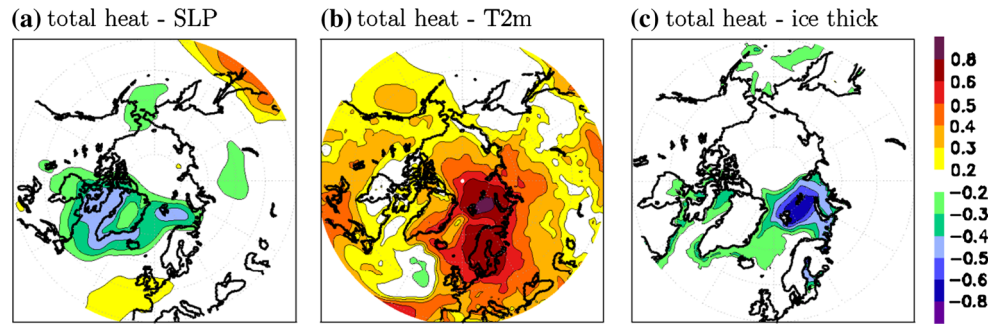


Fig. 5 Correlations between heat transport into the Barents Sea and SLP (a), T2m (b) and sea ice thickness (c) for detrended 11-year running means in the historical simulations, 1850–2005



patterns (Fig. 5). However, while the annual mean Barents Sea heat transport seems to be governed by the anomalous SLP pattern, decadal correlations are highest when the heat transport leads by 0–2 years. Thus, it seems likely that the SLP-reduction in the Iceland region is, at least partly, a response towards enhanced northward heat transport, reduced sea ice and increased SST in the northern North Atlantic. Note, that although the correlation values between SLP and heat transport are higher for 11-year running mean values than for annual mean correlations, the simulated SLP-anomaly is substantially smaller due to relatively small decadal SLP-variations compared to the interannual variability. The correlation with 11-year running mean T2m still shows the highest values in the Barents Sea but the entire northern hemisphere is warm during high heat transport into the Barents Sea. The correlation pattern with 11-year running mean sea ice thickness is similar as for annual mean values. Results from a cross spectrum analysis of the Barents Sea ice volume and the ocean heat transport through the Barents Sea Opening by Koenigk et al. (2009)

indicate that the ocean heat transport is governing the sea ice on decadal time scales.

Figure 6 shows correlations between volume flux driven (V'/T) and temperature driven (T'/V) part of the Barents Sea heat flux and SLP and T2m for time series both with and without trend. The correlation patterns with SLP remain rather unchanged in the twenty first century compared to the twentieth century (Fig. 4a-c): we still find a dipole with negative SLP values around Iceland and over the Greenland Sea and enhanced SLP further south over the North Atlantic and parts of Europe. Also, the correlation is smaller for the temperature driven variations than the velocity driven part at lag 0 but substantially higher when SLP leads by 1 year. We conclude that the processes governing the interannual variations remain the same in future. Furthermore, the trend does not play a dominant role for SLP. This is different for T2m, where the trend clearly dominates the correlation pattern. The correlation of detrended heat transports and T2m values shows similar values in the Barents Sea region and surroundings for the

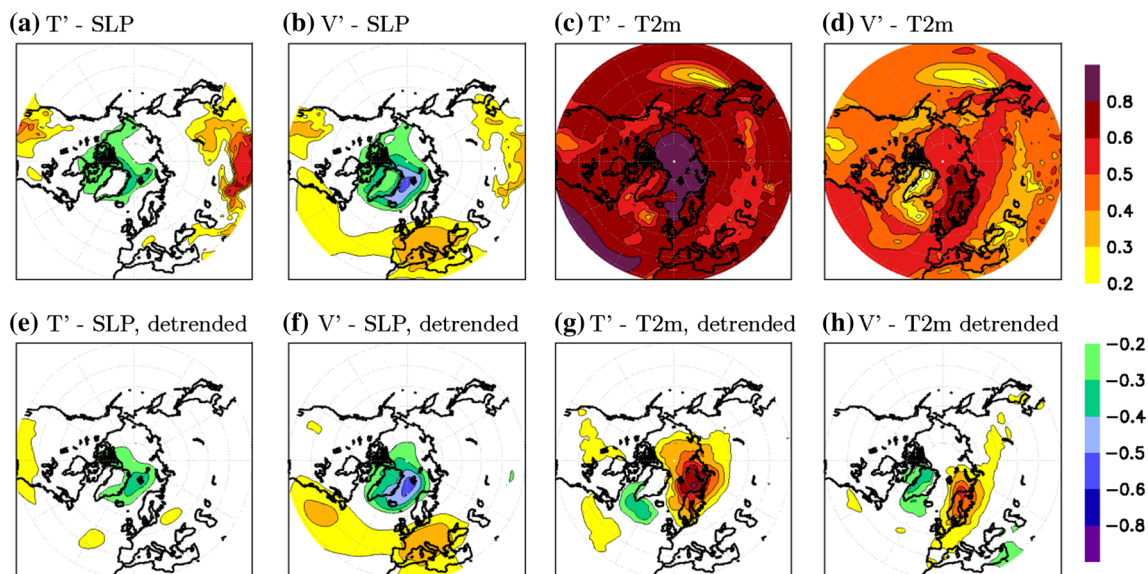


Fig. 6 a Correlation between annual mean heat transport anomalies into the Barents Sea due to temperature anomalies and SLP in the RCP4.5 for the period 2050–2099. b Correlation between heat

transport anomalies due to volume flux anomalies and SLP in RCP4.5, 2050–2099. c and d The same as (a, b) but for T2m. e, f, g, h The same as (a, b, c, d) but for detrended values

temperature driven part as in the twentieth century. However, the area with high correlation extends slightly further to the north into the Central Arctic. The twenty first century correlation pattern of $\overline{V'T}$ and T2m show highest values over northern Scandinavia but much smaller values in the Barents Sea and north of it compared to the twentieth century (compare Figs. 4e, f, 6g, h). The importance of $\overline{V'T}$ for interannual variations of the heat flux into the Barents Sea is reduced in the twenty first century and the correlation pattern with T2m looks like a mainly wind-induced anomaly pattern (Fig. 6h).

3.3 Connection between AMOC and heat transports into the Arctic

The North Atlantic meridional overturning circulation (AMOC) is often used as a monitoring index for the northward heat transport. A strong positive AMOC at a given latitude simply reveals that a lot of dense deep waters are being exported southward, and that this export of water is being balanced by more surface waters flowing northward. A high AMOC at high latitudes is therefore expected to be associated with a high surface northward volume transport into the Arctic. Because these Atlantic surface water masses are relatively warm, one might expect that a strong AMOC episode would be associated with more heat being advected into the Arctic Ocean, giving a positive correlation between AMOC and this heat flux. Levitus et al. (2009) found that observed Barents Sea water temperatures are highly correlated to the Atlantic Multidecadal Oscillation index at multi-decadal time scales. Results by Semenov (2008), based on the global climate model ECHAM5/MPI-OM, showed a significant correlation between Barents Sea inflow and AMOC. On the other hand, recent observations and future model simulations indicate an increase in the northward oceanic heat transport despite a possible reduction of the AMOC. Furthermore,

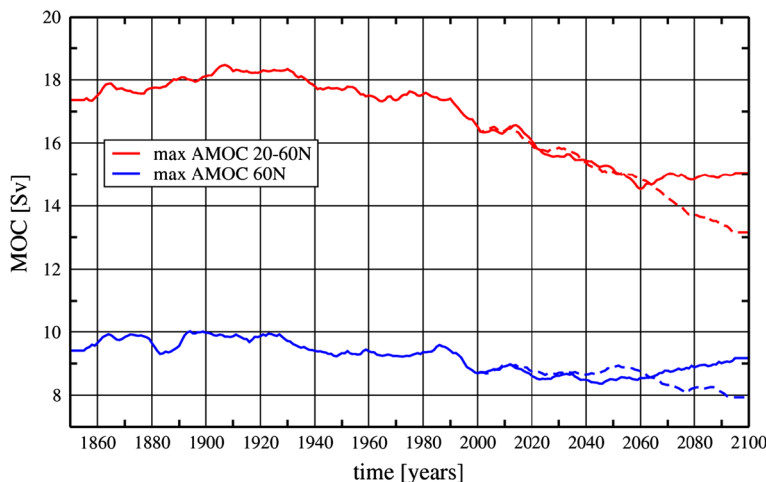
we know from the previous section, that it is the temperature-driven part of the heat flux, and not the volume-driven one, that accounts for most of the increase in the ocean heat transport into the Arctic Ocean.

Here, the meridional overturning circulation is computed as the vertical integration (bottom to surface) of the zonally averaged meridional velocity component. Then, the highest value found in a given range of latitude and depth (between 500 and 2,000 m in our case) is selected as the relevant AMOC index in this study. This index is latitude-dependent and therefore, we separate what we refer to as the maximum of AMOC (found between 20°N and 60°N) from the AMOC at a fixed latitude such as the AMOC at 60°N.

As shown in Fig. 7, EC-Earth sustains an AMOC with a mean maximum value between 17 and 18 Sv during the first 100 years of historical simulation. It starts to significantly and steadily weaken in the second half of the twentieth century to reach a value of 13 Sv in 2100 at the end of the RCP8.5 scenario. In the case of the RCP4.5 scenario, the AMOC stops weakening in the second half of the twenty first century and seems to stabilize around 15 Sv. For the whole period and regardless of the scenarios, the maximum of the AMOC is located typically around 30°N and at a depth of about 800 m (not shown). The mean maximum value for the period 1990–2010 is about 17 Sv. This number compares well with the present-day estimates near 24°N found in the literature: 18 ± 2.5 Sv given by Lumpkin and Speer (2007) and 16 ± 2 Sv found by Ganachaud and Wunsch (2000).

As expected, the AMOC at higher latitudes, 60°N in our case, is weaker and is between 9 and 10 Sv. The same kind of weakening as for the maximum of AMOC is observed, starting in the second half of the twentieth century, but is much less pronounced. At the end of the RCP8.5 scenario, the AMOC at 60°N reaches a minimum of 8 Sv, while the RCP4.5 simulations tend to show a recovery initiated in the

Fig. 7 11-year running mean maximum Atlantic meridional overturning circulation in Sv between 20–60°N (red) and at 60°N (blue) in ensemble means of the RCP4.5 (solid) and the RCP8.5 (dashed) simulations



middle of the twenty first century. The negative trend of the AMOC is in contrast to the increasing trends of the heat transports through the Arctic Straits and indicates that the AMOC is not contributing to the positive trends in the heat transports.

In order to analyze if the AMOC is linked to the natural variability of the heat transports, we calculated correlations between AMOC and heat transports for detrended annual and 11-year running mean values. As a whole, correlations between AMOC and heat transports through the Arctic straits are mostly small. Only heat transports through Fram Strait and the Canadian Archipelago show correlations with the AMOC higher than 0.5 and only for the decadal time scale. No significant correlations are found at inter-annual time-scales.

The highest correlations are found between AMOC and heat transport through Fram Strait at the decadal time scale. They are negative and the highest value, a correlation of -0.73 , is obtained with the AMOC at 60°N for both for the historical (1850–1950) and the RCP4.5 runs (2000–2100). Curiously, the correlation switches sign in the RCP8.5 scenarios (2000–2100) and is $+0.4$.

Regardless of the period and the scenarios studied, the AMOC and the heat transport through the Canadian-Archipelago also show noteworthy positive correlations of about 0.6 and up to 0.7 when the heat flux leads the AMOC by 4 years.

The AMOC is unlikely to be directly related to the heat transports itself, but the wind pattern or the freshwater transport might play the role of the hidden variable responsible for these relatively high correlations. As seen in Sect. 3.2, in both the Canadian Archipelago and the Fram Strait, the heat transport variability is mainly governed by the volume flux, and so is the freshwater flux (Koenigk et al. 2007), which would mean a high correlation between freshwater and heat transport. Heat transports through Fram Strait and Canadian Archipelago are negatively correlated, which is in agreement with the difference of sign in the correlation with AMOC.

As our primary focus is on the Barents Sea, the correlations between the AMOC at different latitudes and the heat and volume fluxes entering the Barents Sea were also extensively investigated. No significant correlations are found; interannual values of the AMOC are just very weakly negatively correlated with the heat transport into the Barents Sea. This tends to prove that the increase of heat transport into the Barents Sea has almost no direct or indirect connections with the intensity of the AMOC, at least in our coupled model.

In contrast to the AMOC, 11-year running means of heat transports through sections across Iceland-Faroe, Iceland-Norway and Greenland-Norway are all positively correlated to the Barents Sea heat transport and largest when the

Barents Sea heat flux lags with 1 year. Warm water masses are transported from the south to the Barents Sea and before reaching the Barents Sea, they also pass the section between Greenland and Norway. This fits well to the relatively high correlation between SLP and the temperature-driven part of Barents Sea heat transport when SLP leads by 1 year (compare Sect. 3.3).

3.4 Heat budget of the Barents Sea

This section discusses the heat budget of the Barents Sea in detail in order to investigate what happens to the increased heat transport after entering the Barents Sea. This area is the region where the scenario simulations with EC-Earth showed by far the largest future climate change in the Arctic (KEA13): the sea ice concentration is strongly reduced in all seasons, annually averaged air temperature increases by up to 15°C , turbulent upward heat fluxes increase by almost 100 W/m^2 , the atmospheric vertical stability is strongly reduced and annual mean precipitation is enhanced by up to 300 mm/year .

Figure 8 shows the boundaries of Barents Sea used in this study directly on the ocean grid. For the sections that are neither zonal nor meridional, the transport of volume and heat are computed across the shortest broken-line connecting the two relevant points (these broken lines are shown in Fig. 8). Therefore, the transport is computed without any velocity interpolation since either the U- or

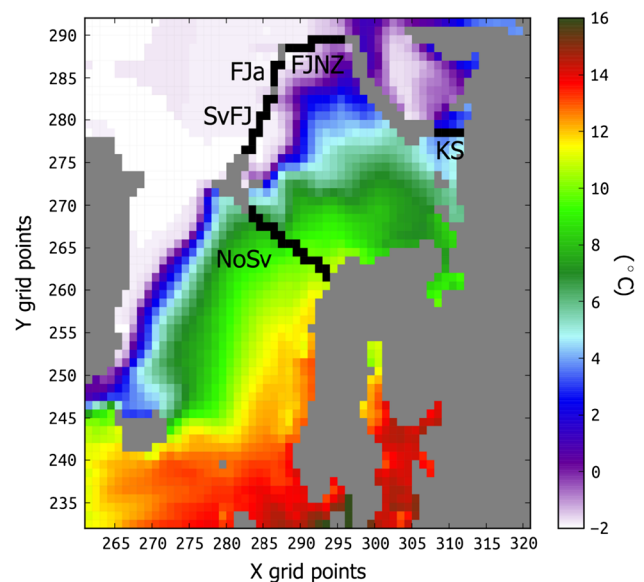


Fig. 8 Monthly SST snapshot (August 2005) directly plotted on the grid of the ocean model for one of the historical simulations used in this study. The *black lines* highlight the grid points defining the 5 lateral boundaries of the Barents Sea domain used for the calculations of mass and heat budget in Sect 3.4: Norway—Svalbard (NoSV), Svalbard—Franz Josef Land (SvFJ), Franz Josef Archipelago (FJa), Franz Josef Land—Novaya Zemlya (FJNZ) and Kara Strait (KS)

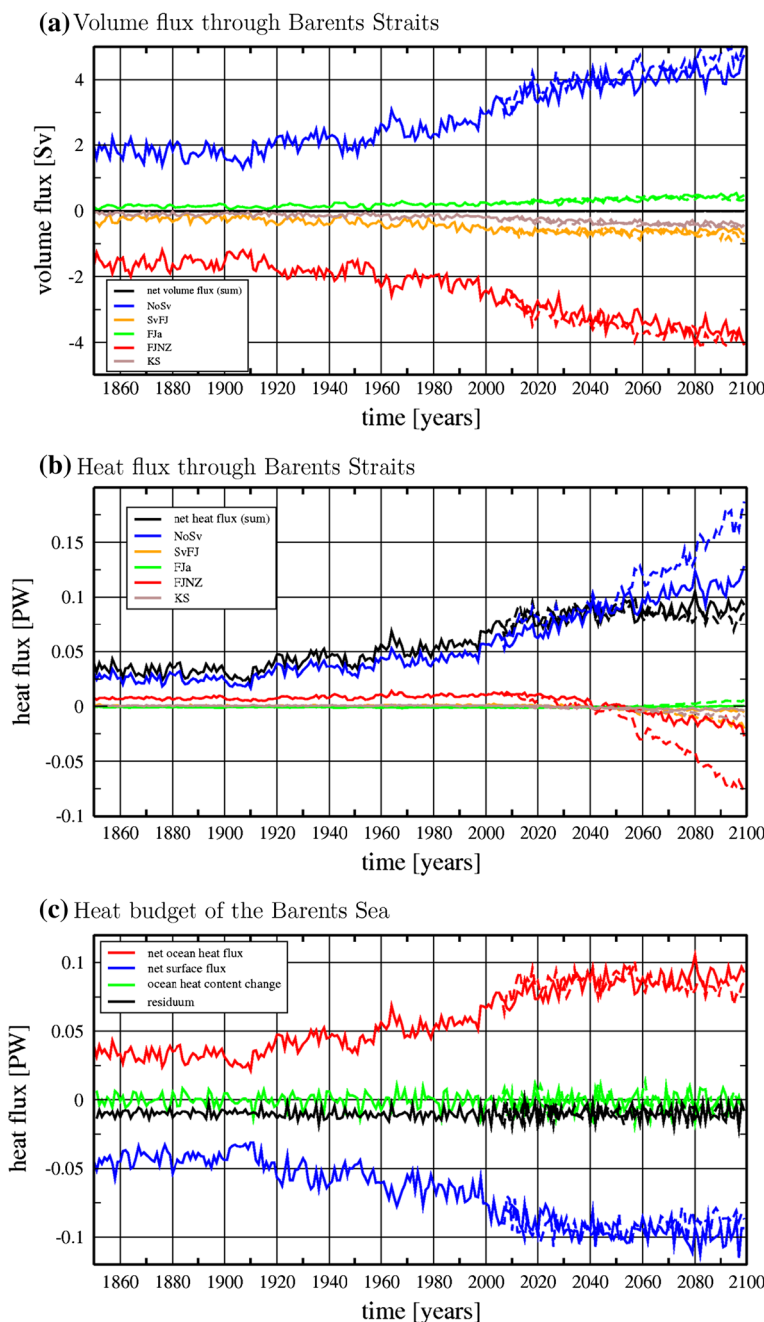
V-component of the velocity is used, depending on the orientation of the local section.

Figure 9a shows that the mass budget in the Barents Sea basin is almost perfectly closed in our simulations. The inflow into the Barents Sea through the Barents Sea Opening is quite stable with about 2 Sv until 1950, thereafter increasing and reaching 3 Sv at year 2000 and 4 Sv at 2040. After 2040, the increase rate declines. Most of the incoming water into the Barents Sea is balanced by exporting water between Franz Josef Land and Novaya Zemlya. In addition, some water is imported through the SvFJ section and exported through the FJa and NZNe

sections. The volume fluxes in our twentieth century simulations agree well with results by Árthun et al. (2012) using a high resolution regional ocean model.

In contrast to the mass balance, the net ocean heat transport into the ocean is not balanced; there is a net flux into the Barents Sea (Fig. 9b, c). This net flux is dominated by the heat transport through the NoSv section and is strongly increasing until about 2050 in the future simulations. The heat transport through the FJNZ section is a source of heat until 2040, but switches sign thereafter and cancels out all further increase in the incoming heat inflow through the Barents Sea Opening. This is valid for all

Fig. 9 **a** Annual mean net ocean volume transport through the openings of the Barents Sea in Sv (for abbreviations see Fig. 8) from 1850 to 2100. Shown are ensemble means of the RCP4.5-simulations (*solid*) and the RCP8.5 simulations (*dashed*). Transports into the Barents Sea are positive. **b** The same as (**a**) but for the net ocean heat transports in PW. **c** Ocean heat budget of the Barents Sea: shown are the net ocean heat transport into the Barents Sea, net surface heat flux, ocean heat content change and the residuum in PW for ensemble means of the RCP4.5 and RCP8.5 simulations. Heat fluxes into the Barents Sea are positive



emission scenarios in EC-Earth. The rapid change in this heat flux can be explained as follows: in the twentieth century, water masses with a temperature below the reference temperature of 0 °C are transported out of the Barents Sea through the FJNZ section, being a source of heat for the Barents Sea. Gradually, temperature increases and comes nearer to Tref, balancing out the increasing export of water masses. After about 2030–2040, the increase of the mass transport slows down while the temperature increase accelerates and temperature passes Tref around 2040, leading to an export of heat out of the Barents Sea.

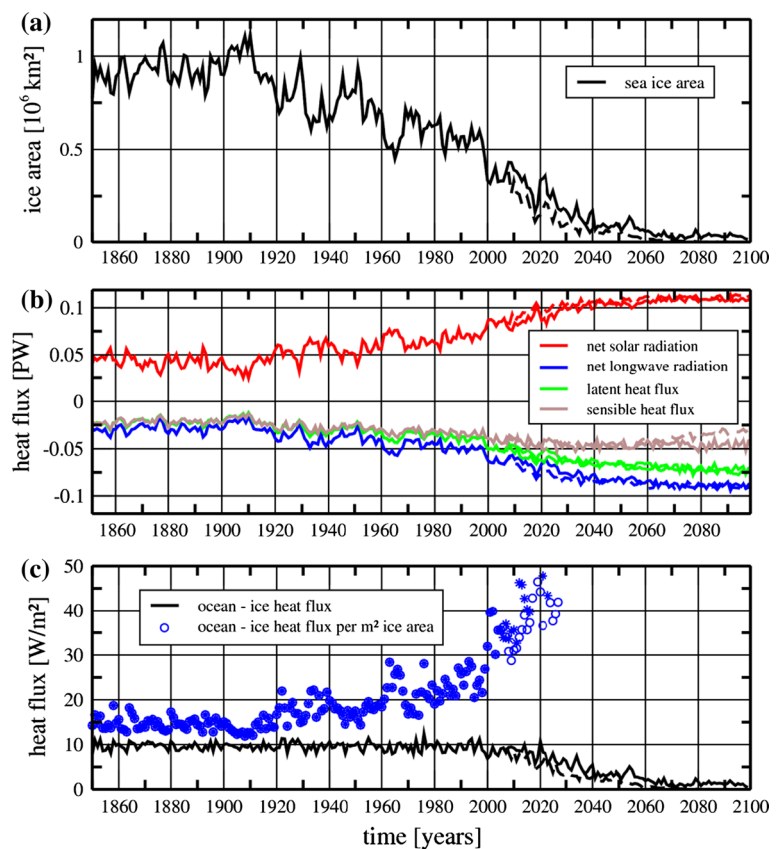
The net ocean heat transport into the Barents Sea is almost balanced by the net surface fluxes in our simulations as shown in Fig. 9c. The time series of annual values are highly anti-correlated and the increase of the net ocean heat transport is balanced by increased surface heat fluxes to the atmosphere in the twenty first century. The ocean heat content shows almost as large interannual variations as the net ocean heat transport and the net surface flux but its change is comparably small, although leading to an increase in the ocean heat content in the twenty first century. The budget is not entirely closed and is negative throughout the entire time period. This imbalance is likely due to processes that we did not take into account like ice transport through the boundaries and river runoff as well as

uncertainties in the calculation due to the use of monthly mean values instead of higher time resolution.

Årthun and Schrum (2010) used a regional coupled ice ocean model for analyzing the heat budget of the Barents Sea (17°E–55°E, 71°N–81°N) in the second half of the twentieth century. They found, similarly to this study, that most of the net ocean heat transport (32TW in their study) is passed to the atmosphere (–34TW), however their values are substantially smaller than ours (about 55TW and –60TW for the same period) and at the lower bound of observational based estimates and model studies (e.g. Mauritzen 1996; Skagseth et al. 2008; Simonsen and Hagan 1996; Årthun et al. 2012).

The time evolution of the surface heat flux components over the open sea area of the Barents Sea together with the Barents Sea ice area and the oceanic heat flux at the ice base are shown in Fig. 10. In the twentieth century, the sea ice area is already strongly reduced and this reduction continues in the twenty first century, leading to almost ice-free conditions year-around in the second half of the twenty first century. Interestingly, the differences between simulations based on the high emission scenario RCP8.5 and those based on the RCP4.5 scenario and the RCP2.6 scenario (not shown in Fig. 10) are relatively small. The net solar surface radiation is strongly increased until the sea ice has vanished in the middle of the twenty first century.

Fig. 10 **a** Annual mean sea ice area of the Barents Sea in 10^6 km^2 in the RCP4.5 (solid) and the RCP8.5 (dashed) simulations. Shown are ensemble means. **b** Annual mean net surface solar radiation, net surface longwave radiation, latent heat flux and sensible heat flux in PW for the open sea area of the Barents Sea in the RCP4.5 (solid) and the RCP8.5 (dashed) simulations. Shown are ensemble means. Fluxes into the ocean are positive. **c** Annual mean ocean heat flux at the ice base in W/m^2 , averaged over the entire Barents Sea domain (black, solid RCP4.5, dashed RCP8.5) and averaged over the ice covered area of the Barents Sea (blue circles, unfilled RCP4.5, filled RCP8.5). Note that the heat flux averaged over the ice area is not shown as soon as the entire Barents Sea is ice-free for at least 1 month in the year. Fluxes into the ice are positive



The net long-wave radiation is becoming larger upwards due to warmer temperatures of the surface in the future simulations and cancels most of the increase in the solar radiation. Latent and sensible surface heat fluxes are both of similar size as the net long-wave radiation in the twentieth century. They are also increasing with reduced ice area until the middle of the twenty first century. However, the increase is less pronounced, particularly for the sensible heat flux. KEA13 showed that the maximum of the sensible heat flux follows northward with the ice edge in the twenty first century, thus leading to increased sensible heat fluxes in the northern part of the Barents Sea but decreased fluxes in the southern part of the Barents Sea. The latent heat flux increases also in the northern part of the Barents Sea due to larger open water areas but does not show any reduction in the southern part of the Barents Sea. The results are rather similar independent of the emission scenario.

The oceanic heat flux at the ice base, averaged over the entire Barents Sea stays constant in the twentieth century, despite reduced ice area, but decreases thereafter (Fig. 10c). However, it is strongly enhanced, particularly from 1980 onwards, if we average over the ice-covered part only. This indicates enhanced bottom melt of the remaining ice in the Barents Sea.

Table 1 shows the correlation coefficients among the heat budget components for annual and 11-year running

mean values of the detrended twentieth century simulations (1850–2005). The absolute values of the correlation coefficients are very high for correlations among all components of the surface heat fluxes and peak at lag 0 or at a lag of 1 year. Note, that the differences in correlations between consecutive lags are not significant in most cases, particularly not for the 11-year running mean values, where autocorrelations are high for lags up to a few years. All heat flux components are highly correlated to the sea ice area, which seems to govern all the surface heat fluxes: reduced ice area leads to more open water and higher temperature in the Barents Sea, thus increasing upward fluxes of latent and sensible heat and longwave radiation, and the reduced ice area allows for more absorption of solar radiation due to reduced surface albedo.

The sea ice area itself seems to be led by the net ocean heat transport into the Barents Sea and the oceanic heat flux at the ice base. As discussed in Sect. 3.2, variations of the sea ice transport into the Barents Sea are playing an important role for the ice area in the Barents Sea as well at interannual time scales. Large ice transports into the Barents Sea are related to northerly winds, which at the same time reduce the ocean heat transport by cooling water and reducing the volume transport from the south.

Table 1 Correlations among detrended heat components of the Barents dsSea heat budget for 1850–2005: annual means (top right corner, bold) and 11-year running mean (bottom left corner)

1-y mean/11-y mean	SIA	OHTnet	SHFnet	SWsurf net	LWsurf net	SHF	LHF	O-I HF
SIA	1	-0.74 (0) -0.68 (-1)	0.78 (0) 0.76 (1)	-0.97 (0)	0.98 (0)	0.80 (0) 0.74 (1)	0.96 (0)	-0.67 (-1) -0.63 (0)
OHTnet	-0.93 (1) -0.91 (0)	1	-0.79 (1)	0.67 (0) 0.64 (1)	-0.72 (0) -0.72 (1)	-0.76 (1)	-0.76 (1) -0.73 (0)	0.64 (1)
SHFnet	-0.97 (0) -0.96 (1)	-0.97 (-1) -0.96 (0)	1	-0.73 (0) -0.69 (-1)	0.84 (0)	0.96 (0)	0.91 (0)	-0.76 (0)
SWsurf net	-0.99 (0)	0.92 (0) 0.91 (-1)	-0.96 (0)	1	-0.68 (0) -0.66 (1)	-0.73 (0)	-0.94 (0)	0.61 (0)
LWsurf net	0.99 (0)	-0.94 (0) -0.94 (-1)	0.97 (0)	-0.99 (0)	1	0.85 (0)	0.98 (0)	-0.68 (0) -0.67 (1)
SHF	0.96 (0) 0.95 (-1)	-0.94 (-1) -0.93 (0)	0.98 (0)	-0.96 (0) -0.95 (-1)	0.96 (0) 0.94 (-1)	1	0.91 (0)	-0.73 (0)
LHF	0.99 (0)	-0.95 (0) -0.95 (-1)	0.99 (0)	-0.98 (0)	0.99 (0)	0.97 (0) 0.96 (1)	1	-0.72 (0)
O-I HF	-0.71 (0) -0.70 (1)	0.81 (0)	-0.74 (0) -0.74 (1)	0.73 (0)	-0.75 (0) -0.74 (1)	-0.68 (0) -0.68 (1)	-0.77 (0) -0.76 (1)	1

In parenthesis, the lag in years of the highest correlations is shown; in case the correlation is similar at different lag-times, both correlations-coefficients are presented (positive lags mean that the variable in the horizontal is leading, negative means that the variable in the vertical is leading). SIA sea ice area, OHTnet net ocean heat transport, SHFnet net surface heat flux, SWsurf net net surface solar radiation, LWsurf net net surface long wave radiation, SHF sensible heat flux, LHF latent heat flux, O-I HF ocean to sea ice heat flux

3.5 Impact of increased ocean heat transport on the Central Arctic Ocean

The question if enhanced ocean heat transport will directly affect sea ice melt in the Central Arctic Ocean is of large importance for the future development of Arctic sea ice. Here, we analyze vertical sections in the Arctic Ocean and the oceanic heat flux at the ice base. We aim to find out if the stratification and vertical processes in the Arctic Ocean change and allow for a direct contact of the warm inflowing water masses with the sea ice in the Central Arctic Ocean in the future simulations.

The oceanic heat flux at the ice base is largest along the ice edges where ice is either transported southward towards relatively warm water masses as in the East Greenland Current and in the Labrador Sea or warm water masses are transported towards the ice edge as in the Barents Sea (Fig. 11, shown are the heat fluxes for the ice covered part in each grid box). Areas with largest bottom melt are displaced towards the north with the ice edge in the future simulations. At the same time, the area with bottom melt extends from the Barents Sea along the Siberian coast and to a smaller degree also from the Bering Strait along both the North American and Siberian coast. The area of increased basal ice heat fluxes extends gradually further into the Central Arctic.

Increased melting from below is not necessarily caused by enhanced ocean heat transport into the Arctic. It could also be due to more energy input into the upper ocean from the atmosphere. However, since latent and sensible heat fluxes are growing upward in the entire Arctic (see KEA13, Fig. 5), radiation would be the only possible source of heat.

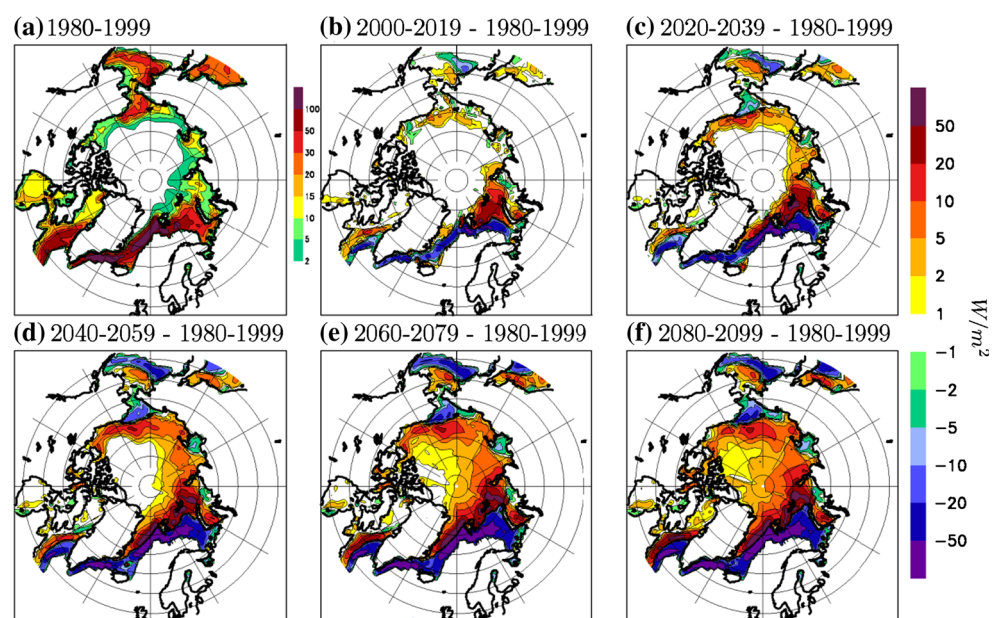
Although the net surface radiation is slightly increased in most of the Arctic in the twenty first century (not

shown), the pattern differs substantially from the change pattern of the heat flux at the ice base. Also, the net surface radiation increase is too small to explain the entire increase in the basal ice heat flux in the Barents Sea and north of it. However, in the Central Arctic, the changes in net surface radiation are of similar size as the changes in the ocean to ice heat flux and might be the major source for increased bottom melt of sea ice.

To analyze the path of the inflowing warm water in EC-Earth in the twentieth and twenty first century, we analyzed vertical sections (Fig. 12). At the end of the twentieth century, the inflowing Atlantic water has a temperature of about 4 °C at 72°N in the Barents Sea. As soon as the water advances to the ice edge it is strongly cooled and mixed down to larger depth forming a warm intermediate layer. Compared to observations and climatological values (Locarnini et al. 2010), this layer occurs in the right depth of about 500 m but the vertical temperature gradients connected to this warm layer are not sufficiently pronounced in EC-Earth. The ocean below the intermediate layer is too warm. The Atlantic water is mixed too fast into the deep ocean in our model since it is slightly too dense due to too cold temperatures and slightly overestimated salinity. Similar characteristics of the Arctic water masses are also found in the CCSM4 global model (Jahn et al. 2012).

Summer and winter conditions differ quite a lot from each other (Fig. 13a, b). In winter, the northward transported water is cooled by heat release to the atmosphere, sinks down and forms the warm intermediate Atlantic layer. In summer, the upper 50 m are strongly warmed in the Barents Sea and no formation of intermediate Arctic water occurs. The intermediate water layer formed in winter survives summer but is somewhat less pronounced

Fig. 11 **a** Annual mean ocean heat flux at the ice base averaged over 1980–1999 in W/m^2 . Shown is the ensemble mean. Positive values show heat fluxes from the ocean into the ice. **b** Changes in annual mean ocean heat flux at the ice base between the periods 2000–2019 and 1980–1999 in W/m^2 . Shown are ensemble means of the RCP4.5 simulations. **c** The same as **(b)** but for 2020–2039. **d** The same as **(b)** but for 2040–2059. **e** The same as **(b)** but for 2060–2079. **f** The same as **(b)** but for 2080–2099



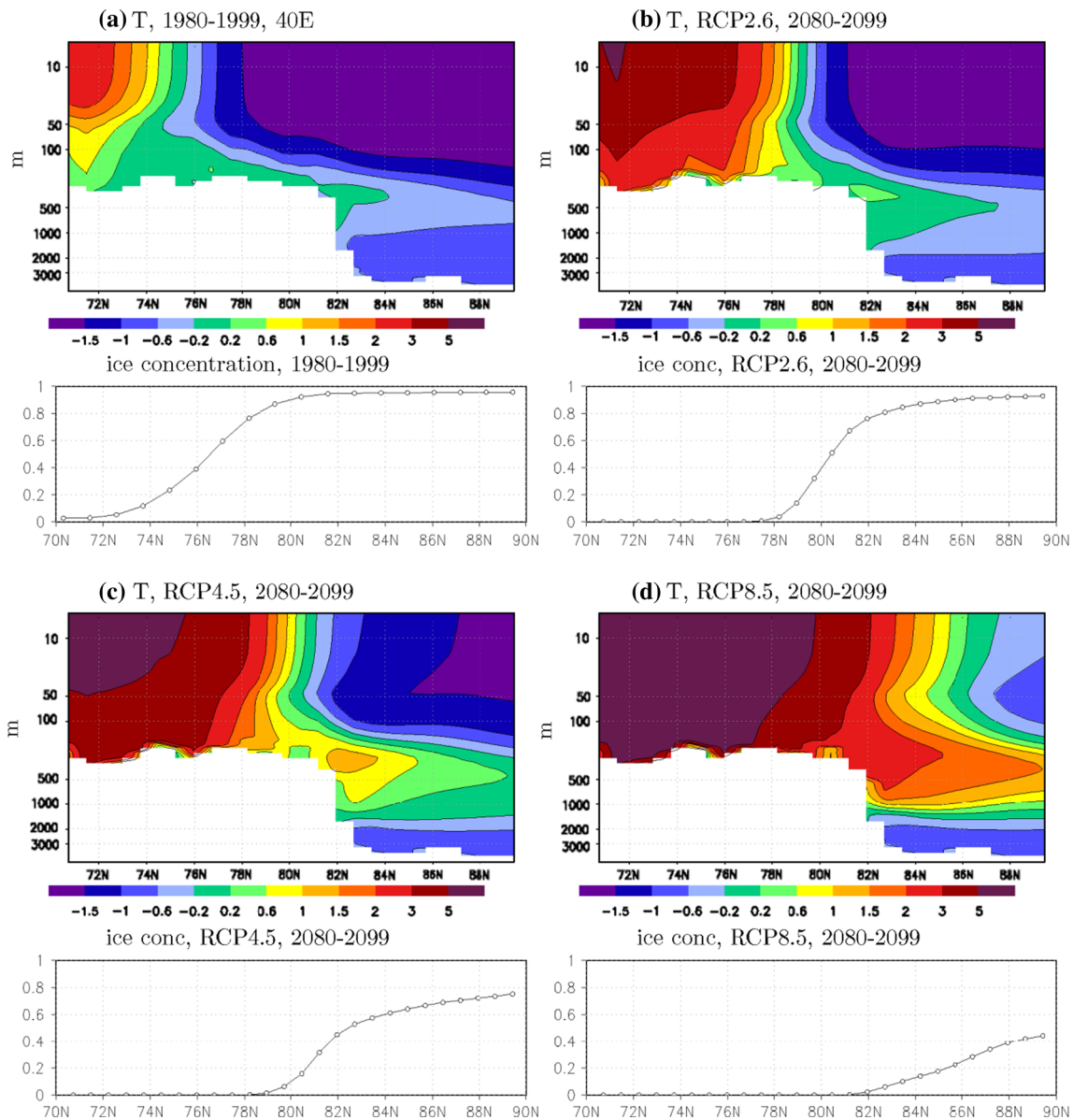


Fig. 12 **a** Temperature profile and sea ice concentrations along 40°E, 70–90°N for annual mean values averaged over 1980–1999. Shown are ensemble means. **b** The same as (a) but for the period 2080–2099

in RCP2.6. **c** The same as (a) but for 2080–2099 in RCP4.5. **d** The same as (a) but for 2080–2099 in RCP8.5

than in winter. Between this intermediate layer and the surface layer, a tongue of colder water extends to the south. The warm surface waters penetrate further northward into partly ice covered regions compared to the winter.

At the end of the twenty first century, the incoming Atlantic water masses are substantially warmer and extend much further to the north (Fig. 13c, d). This goes along with a displacement of the ice edge to the north. Still, strong cooling and downward mixing occur at the ice edge in RCPs 2.6 and 4.5 and Arctic intermediate water is formed in winter. The temperature gradient near the ice edge is strengthened in winter related to a more rapid transition from ice-free conditions to nearly totally ice

covered conditions. In summer, the upper surface layer is warmed in the Barents Sea and, similar to the end of the twentieth century, this warm layer is separated from the warm intermediate water by a layer of cold water, which extends to the south. This layer is increasingly pronounced at the end of the twenty first century. Also, the intermediate water layer is strengthened, which is in agreement to results by Karcher et al. (2003, 2011) showing that recent pulses of warm Atlantic water lead to a more pronounced intermediate layer of Atlantic water in the Arctic Ocean.

In our RCP8.5 simulations, we see a strong warming at all depths above 1,500 m with the largest warming at the surface. Annual mean sea ice concentration is low along the

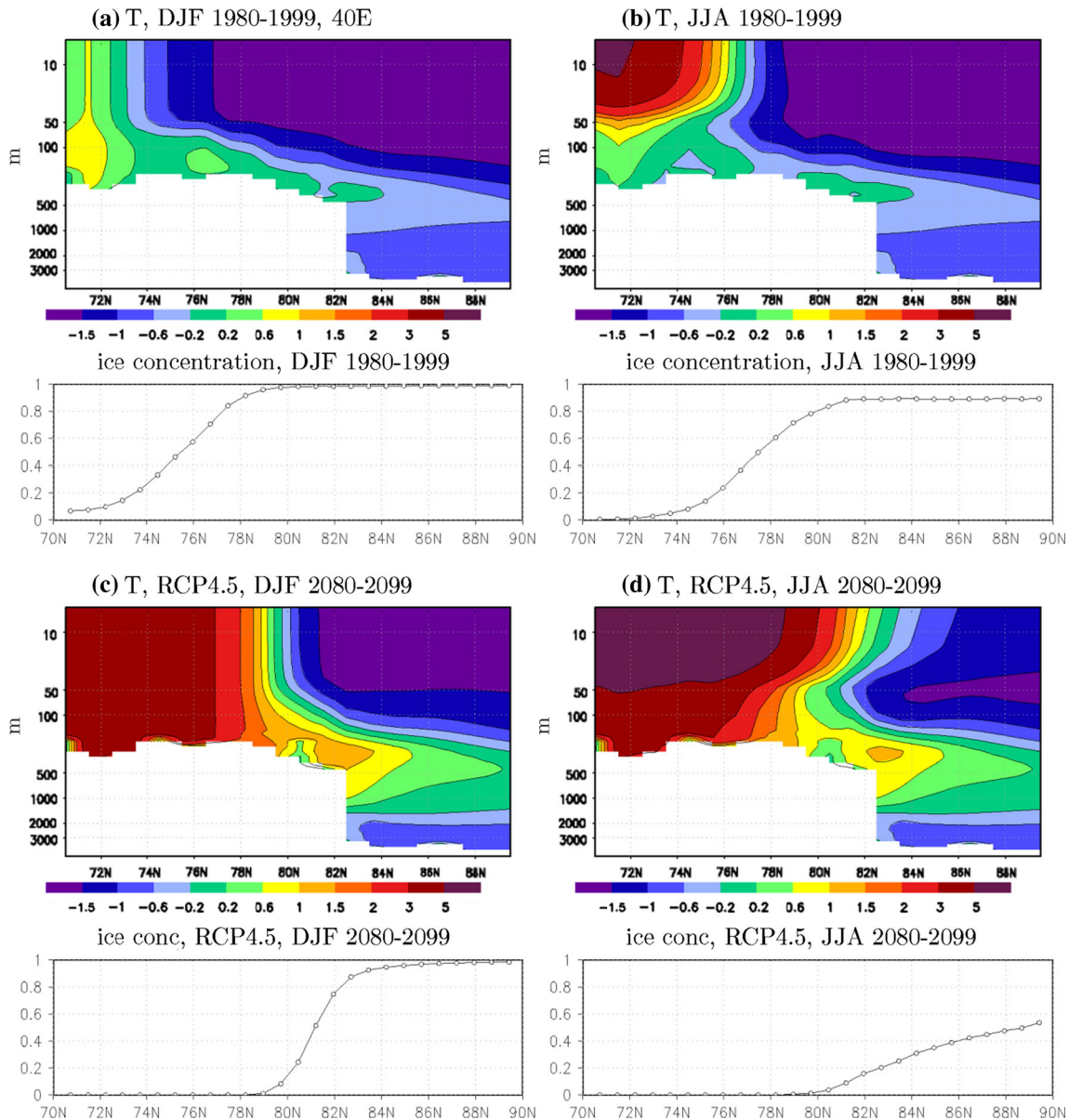


Fig. 13 Temperature profile and sea ice concentrations along 40°E, 70–90°N for winter (DJF, **a**, **c**) and summer (JJA, **b**, **d**) mean values averaged over 1980–1999 (**a**, **b**) and over 2080–2099 in RCP4.5 (**c**, **d**). Shown are ensemble means

entire section, indicating an ice-free summer and autumn. The surface waters can thus warm up during summer and might penetrate further into ice covered regions and thus extend the area of bottom melt as seen in Fig. 11.

None of the scenario simulations indicate a general change in processes and there is no indication for enhanced bottom melt in the interior of the Arctic due to enhanced ocean heat transport through the Barents Sea. The heat from the incoming warm water is either passed to the atmosphere, increases ice melt near the ice edge or warms the intermediate layer.

The inflowing water masses through Bering Strait are substantially warmed as well in the twenty first century

(Fig. 14). The warm water is well mixed over the entire depth of the shallow Bering Strait. The horizontal temperature gradient at the ice edge is smaller and annual mean ice concentration is more gradually increasing to the north than in the Barents Sea. This is due to larger variations of the ice edge between summer and winter in this area compared to the Barents Sea. In the twenty first century simulations, the warm water extends further to the north and, in contrast to Barents Sea, it remains near the surface. Thus, it is potentially contributing to enhanced bottom ice melt. An increase of 1 Watt in the ocean heat transport through the Bering Strait contributes probably more efficiently to bottom ice melt than the same increase

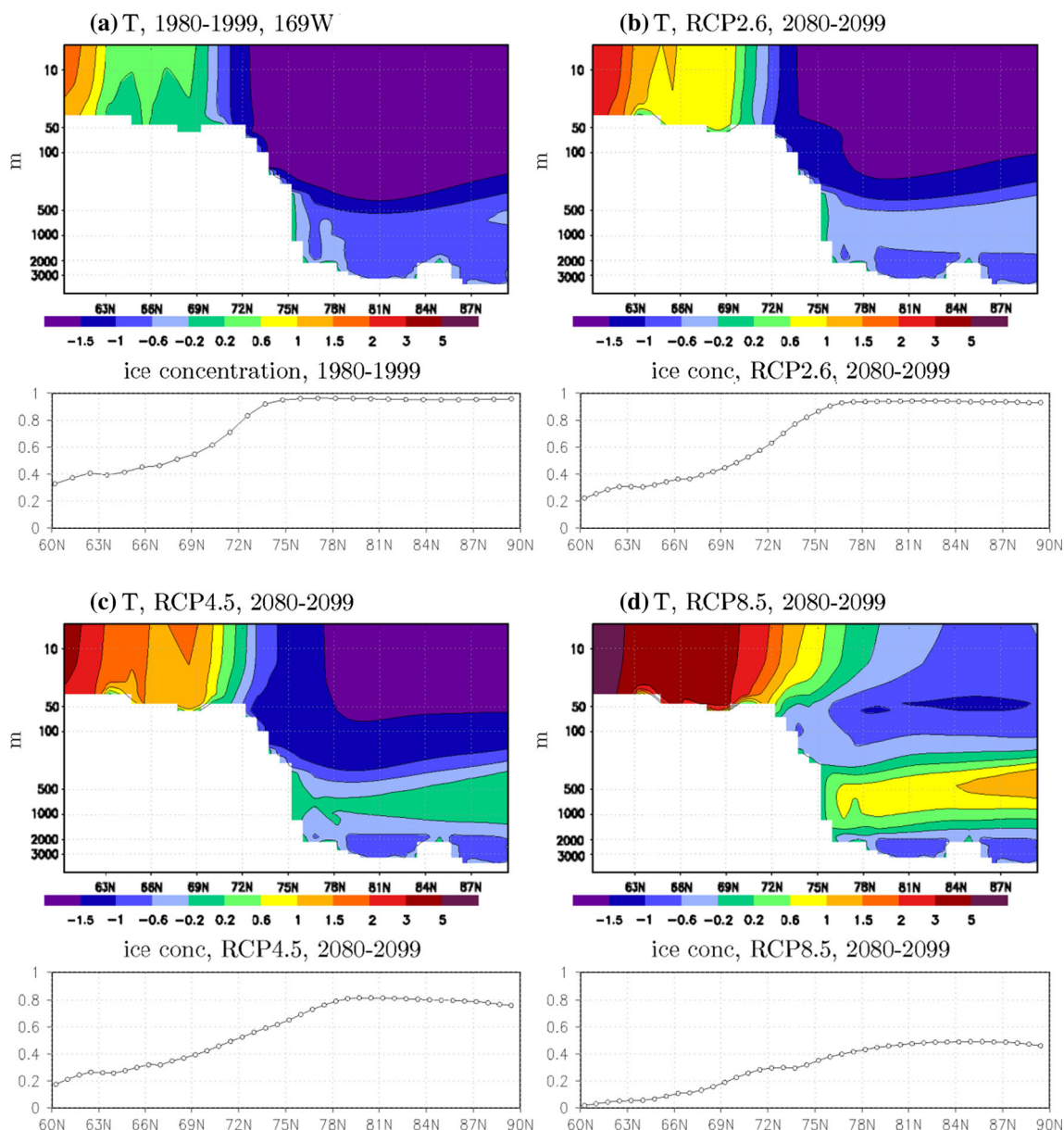


Fig. 14 **a** Temperature profile and sea ice concentrations along 169°W, 60–90°N for annual mean values averaged over 1980–1999. Shown are ensemble means. **b** The same as (a) but for the period

2080–2099 in RCP2.6. **c** The same as (a) but for 2080–2099 in RCP4.5. **d** The same as (a) but for 2080–2099 in RCP8.5

in the heat transport into the Barents Sea. However, we have to keep in mind that the increase in ocean heat transport into the Barents Sea is about one order of magnitude larger than that through the Bering Strait.

4 Conclusions

This study analyzed the ocean heat transport into the Arctic in the twentieth and twenty first century in an ensemble of future scenario simulations based on the CMIP5 emission scenarios with the global coupled climate model EC-Earth.

The heat transport to the north simulated in EC-Earth compares relatively well to observational based estimates.

At 70°N, the atmospheric heat transport is one order of magnitude larger than the ocean heat transport but decadal variations are of similar size. Often the decadal variations are partly or totally canceling each other (Bjerknes compensation); the correlation between 11-year running mean of oceanic and atmospheric northward heat transport is -0.72 when the ocean leads by 2 years. The atmospheric heat transport across 70°N is reduced by 0.05PW and 0.15PW until the end of the twenty first century in RCP2.6 and RCP8.5, respectively. The transport in the ocean is

enhanced by almost exactly the same numbers. The Bjerknes compensation remains nearly unchanged in scenario simulations of the twenty first century.

Variations of the heat transports through the Barents Sea Opening and through Bering Strait are governed by both temperature and volume flux anomalies in the heat transports while the transports through Fram Strait and the Canadian Archipelago are mainly dominated by variations in the volume flux. In the twenty first century, the ocean heat transport into the Arctic is strongly growing mainly due to a strong increase in the heat transport into the Barents Sea. This increase is mainly caused by warming of the northward flowing Atlantic water masses. Variations in the ocean heat transport into the Barents Sea are both in the twentieth and twenty first century related to a NAO+ like SLP pattern together with an enhanced SLP gradient across the Barents Sea Opening. This leads to more south-westerly winds over the Nordic Seas and enhances the volume transport and advects warmer water northward towards the Barents Sea.

On decadal time-scales, the heat transport into the Barents Sea seems to lead the SLP by about 1 year indicating a feedback on the SLP from the reduced ice and the warmer SST. The correlations of oceanic heat transport with ice thickness and air temperature are largest in the Barents Sea/Kara Sea region and the correlation patterns agree well with the climate change patterns in future scenario simulations by Koenigk et al. (2013). The relation between AMOC and heat and volume fluxes through the Arctic Straits is small and trends are of opposite sign in the twenty first century.

A large fraction of the enhanced oceanic heat transport into the Barents Sea is passed to the atmosphere and warms the atmosphere. The increased heat transport leads also to enhanced heat fluxes at the ice base and contributes to reduced ice area. The reduced sea ice is strongly governing the changes in surface heat fluxes in the Barents Sea by more open sea, enhanced surface temperature and reduced surface albedo. Latent and sensible heat fluxes are increased. The net surface solar radiation is enhanced downward and the net longwave radiation upward, almost canceling each other.

The heat release to the atmosphere in the Barents Sea cools the incoming Atlantic warm water masses, which increase the density and lead to the formation of a warm intermediate layer of Atlantic water in the Arctic. This intermediate layer has no contact to the surface and thus a minor impact on sea ice and atmosphere in the Central Arctic. In the future scenarios, the temperature of the incoming Atlantic water increases and the warm water moves further into the Arctic together with the northward moving ice edge. However, most of the Atlantic warm water is still cooled after advancing to the ice edge and

forms a much more pronounced intermediate layer of Atlantic water in the Arctic compared to the twentieth century. From about 2050 onwards, sea ice has almost totally melted in the Barents Sea. As a consequence, surface heat fluxes are not changing much any longer. The increase of ocean heat inflow through the Barents Sea Opening is compensated by enhanced heat outflow between Franz Josef Land and Novaya Zemlya. Our model results show also increased bottom ice melt in the Central Arctic but most likely, this is due to increased net surface radiation input into the upper ocean.

The warm water transported through the Bering Strait into the Arctic has a lower salinity than the Atlantic water and is thus staying near the surface. Consequently, the increase in ocean heat transport through the Bering Strait is more directly increasing sea ice melt at the ice base than the heat transport into Barents Sea, however, the increase in heat transport through the Bering Strait is much smaller.

The northward heat transport into the Arctic differs strongly between the different emission scenarios with much larger increase in the high emission scenarios. In addition, relatively large differences can be seen between simulations using the same emission scenario on decadal scales. This clearly indicates uncertainties in the change signal due to natural variability. An ensemble of three as used in this study is not sufficiently large to capture the entire uncertainty due to natural variability. However, general, the common change signal and the differences between the emission scenarios are by far larger than the natural variability of the heat transports. Interestingly, the responses of ocean heat release and net ocean heat transport in the Barents Sea do not strongly depend on the emission scenario. This strengthens results by Koenigk et al. (2013) indicating that the future climate response in the Barents Sea is less sensitive to the emission scenario than other high-latitude regions.

Acknowledgments This study has been made possible by support of the Rossby Centre at the Swedish Meteorological and Hydrological Institute (SMHI) together with the Swedish Research Council Formas financed project ADSIMNOR.

Open Access This article is distributed under the terms of the Creative Commons Attribution License which permits any use, distribution, and reproduction in any medium, provided the original author(s) and the source are credited.

References

- Aagaard K, Coachman LK, Carmack E (1981) On the halocline of the Arctic Ocean. *Deep Sea Res* 28A(6):529–545
- ACIA (2005) Arctic climate impact assessment. Cambridge University Press, Cambridge, p 1042

- Ådlandsvik B, Loeng H (1991) A study of the climatic system in the Barents Sea. *Polar Res* 10(1):45–49
- Aksenov Y, Bacon S, Coward AC, George Nurser AJ (2010) The North Atlantic inflow into the Arctic Ocean: high-resolution model study. *J Mar Syst* 79:1–22. doi:10.1016/j.jmarsys.2009.05.003
- Årthun M, Schrum C (2010) Ocean surface heat flux variability in the Barents Sea. *J Mar Syst* 83:88–98
- Årthun M, Eldevik T, Smedsrud LH, Skagseth Ø, Ingvaldsen RB (2012) Quantifying the influence of Atlantic heat on Barents Sea ice variability and retreat. *J Clim* 23:4736–4743. doi:10.1175/Jcli-D-1100466.1
- Balsamo G, Viterbo P, Beljaars A, van den Hurk B, Betts A, Scipal K (2009) A revised hydrology for the ECMWF model: verification from field site to terrestrial water storage and impact in the integrated forecast system. *J Hydrometeorol* 10:623–643
- Bechtold P, Köhler M, Jung T, Leutbecher M, Rodwell M, Vitart F, Balsamo G (2008) Advances in predicting atmospheric variability with the ECMWF model, 2008: from synoptic to decadal time-scales. *Quart J Roy Meteor Soc* 134:1337–1351
- Bengtsson L, Semenov VA, Johannessen OM (2004) The early twentieth-century warming in the arctic—a possible mechanism. *J Clim* 17:4045–4057
- Bjerknes J (1964) Atlantic air-sea interaction. *Advances in geophysics* 10. Academic Press, London, pp 1–82
- Bouillon S, Morales Maqueda MA, Legat V, Fichetef T (2009) An elastic-viscous-plastic sea ice model formulated on Arakawa B and C grids. *Ocean Model* 27(3–4):174–184. doi:10.1016/j.ocemod.2009.01.004
- Comiso JC, Parkinson C, Gersten R, Stock L (2008) Accelerated decline in the Arctic sea ice cover. *Geophys Res Lett* 35(L01703). doi:10.1029/2007GL031972
- Dickson RR, Osborn TJ, Hurrell JW, Meincke J, Blindheim J, Ådlandsvik B, Vinje T, Alekseev G, Maslowski W (2000) The Arctic Ocean response to the North Atlantic Oscillation. *J Clim* 13:2671–2696
- Dmitrenko IA, Polyakov IV, Krillov SA, Timokhov LA, Frolov IE, Sokolov VT, Simmons HL, Ivanov VV, Walsh D (2008) Toward a warmer Arctic Ocean: spreading the early 21st century Atlantic Water warm anomaly along the Eurasian Basin margins. *J Geophys Res* 113:C05023. doi:10.1029/2007JC004158
- Dutra E, Balsamo G, Viterbo P, Miranda PMA, Beljaars A, Schär C, Elder K (2010) An improved snow scheme for the ECMWF land surface model: description and offline validation. *J Hydrometeorol* 11:899–916. doi:10.1175/2010JHM1249.1
- Fichetef T, Morales Maqueda MA (1997) Sensitivity of a global sea ice model to the treatment of ice thermodynamics and dynamics. *J Geophys Res* 102(C6):609–612. doi:10.1029/97JC00480
- Furevik T (2001) Annual and interannual variability of Atlantic Water temperatures in the Norwegian and Barents Seas: 1980–1996. *Deep Sea Res* 48:383–404
- Ganachaud A, Wunsch C (2000) Improved estimates of global ocean circulation, heat transport and mixing from hydrographic data. *Nature* 408:453–457
- Goosse H, Holland M (2005) Mechanisms of decadal arctic climate variability in the community climate system model, version 2 (CCSM2). *J Clim* 18:3552–3570
- Goosse H, Selten FM, Haarsma RJ, Opsteegh JD (2003) Large sea-ice volume anomalies simulated in a coupled climate model. *Clim Dyn* 20:523–536. doi:10.1007/s00382-002-0290-4
- Graversen RG, Wang M (2009) Polar amplification in a coupled climate model with locked albedo. *Clim Dyn* 33:629–643. doi:10.1007/s00382-009-0535-6
- Graversen RG, Mauritsen T, Tjernström T, Källén E, Svensson G (2008) Vertical structure of recent Arctic warming. *Nature* 454:541. doi:10.1038/nature06502
- Häkkinen S, Cavalieri DJ (1989) A study of oceanic surface heat fluxes in the Greenland, Norwegian and Barents Sea. *J Geophys Res* 94:6145–6157
- Hazeleger W, Severijns C, Semmler T, Stefanescu S, Yang S, Wang X, Wyser K, Baldasano JM, Bintanja R, Bougeault P, Caballero R, Dutra E, Ekman AML, Christensen JH, van den Hurk B, Jimenez P, Jones C, Källberg P, Koenigk T, MacGrath R, Miranda P, van Noije T, Schmith T, Selten F, Storelvmo T, Sterl A, Tapamo H, Vancoppenolle M, Viterbo P, Willén U (2010) EC-earth: a seamless earth system prediction approach in action. *Bull Am Meteor Soc* 91:1357–1363. doi:10.1175/2010BAMS2877.1
- Hazeleger W, Wang X, Severijns C, Stefanescu S, Bintanja R, Sterl A, Wyser K, Semmler T, Yang S, van den Hurk B, van Noije T, van der Linden E, van der Wiel K (2012) EC-EarthV2: description and validation of a new seamless Earth system prediction model. *Clim Dyn*. doi:10.1007/s00382-011-1228-5
- Hopkins TP (1991) The GIN sea—a synthesis of its physical oceanography and literature review. *Earth Sci Rev* 30:175–319
- Ikeda M (1990) Decadal oscillations of the air-ice-ocean system in the northern hemisphere. *Atmos Ocean* 28(1):106–139
- IPCC (2007) Climate change 2007: the physical science basis. In: Solomon S, Qin D, Manning M, Chen Z, Marquis M, Averyt KB, Tignor M, Miller HL (eds) Contribution of working group I to the fourth assessment report of the intergovernmental panel on climate change. Cambridge University Press, Cambridge
- Jahn A, Sterling K, Holland MM, Kay JE, Maslanik JA, Bitz CM, Bailey DA, Stroeve J, Hunke EC, Lipscomb WH, Pollak DA (2012) Late-twentieth-century simulation of arctic sea ice and ocean properties in the CCSM4. *J Clim* 25:1431–1452. doi:10.1175/JCLI-D-11-00201.1
- Jungclauss JH, Koenigk T (2010) Low-frequency variability of the Arctic climate: the role of oceanic and atmospheric heat transport variations. *Clim Dyn* 34(2–3):265–279. doi:10.1007/s00382-009-0569-9
- Karcher MJ, Gerdes R, Kauker F, Köberle C (2003) Arctic warming: evolution and spreading of the 1990s warm event in the Nordic seas and the Arctic Ocean. *J Geophys Res* 108(C2). doi:10.1029/2001JC001265
- Karcher MJ, Beszczynska-Möller A, Kauker F, Gerdes R, Heyen S, Rudels B, Schauer U (2011) Arctic Ocean warming and its consequences for the Denmark Strait overflow. *J Geophys Res* 116:C02037. doi:10.1029/2010JC006265
- Koenigk T, Mikolajewicz U, Haak H, Jungclauss J (2007) Arctic freshwater export in the 20th and 21st century. *J Geophys Res* 112. doi:10.1029/2006JG000274
- Koenigk T, Mikolajewicz U, Jungclauss J, Kroll A (2009) Sea ice in the Barents Sea: seasonal to interannual variability and climate feedbacks in a global coupled model. *Clim Dyn* 32:1119–1138. doi:10.1007/s00382-008-0450-2
- Koenigk T, Brodeau L, Graversen RG, Karlsson J, Svensson G, Tjernström M, Willén U, Wyser K (2013) Arctic climate change in 21st century CMIP5 simulations with EC-Earth. *Clim Dyn* 40(11):2719–2743. doi:10.1007/s00382-012-1505-y
- Levitus S, Matishov G, Seidov D, Smolyar I (2009) Barents Sea multidecadal variability. *Geophys Res Lett* 36(L19604). doi:10.1029/2009GL039847
- Liu Y, Key JR, Wang X (2008) The influence of changes in cloud cover on recent surface temperature trends in the Arctic. *J Clim* 21:705–715
- Locarnini RA, Mishonov AV, Antonov JJ, Boyer TP, Garcia HE, Baranova OK, Zweng MM, Johnson DR (2010) World Ocean Atlas 2009, volume 1: temperature. In: Levitus S (ed) NOAA Atlas NESDIS 69. U.S Government Printing Office, Washington, DC
- Lumpkin R, Speer K (2007) Global ocean meridional overturning. *J Phys Oceanogr* 37:2550–2562

- Madec G (2008) “NEMO ocean engine”. Note du Pole de modélisation, Institut Pierre-Simon Laplace (IPSL), France, No 27 ISSN No 1288-1619
- Mauritzen C (1996) Production of dense overflow waters feeding the North Atlantic across the Greenland-Scotland Ridge. Part 2: an inverse model. *Deep Sea Res* 1(43):807–835
- Melling H, Agnew TA, Falkner KK, Greenberg DA, Lee CM, Münchow A, Petrie B, Prinsenberg SJ, Samelson RM, Wodgate RA (2008) Fresh-Water Fluxes via Pacific and Arctic Outflows Across the Canadian Polar Shelf. In: Dickson B, Meincke J, Rhines P (eds) *Arctic-Subarctic ocean fluxes: defining the role of Nordic Seas in climate*, Chap 9. Springer, Berlin
- Münchow A, Melling H (2008) Ocean current observations from Nares Strait to the west of Greenland: interannual to tidal variability and forcing. *J Mar Res* 66(6):801–833
- Oliver KE, Heywood KJ (2003) Heat and freshwater fluxes through the Nordic Seas. *J Phys Oceanogr* 33:1009–1026
- Orvik KA, Skagseth Ø (2005) Heat flux variations in the eastern Norwegian Atlantic Current toward the Arctic from moored instruments, 1995–2005. *Geophys Res Lett* 32(L14610). doi:[10.1029/2005GL023487](https://doi.org/10.1029/2005GL023487)
- Polyakov IV, Alekseev GV, Timokhov LA, Bhatt US, Colony RL, Simmons HL, Walsh D, Walsh JE, Zakharov VF (2004) Variability of the Intermediate Atlantic Water of the Arctic Ocean over the Last 100 Years. *J Clim* 17(23):4485–4497
- Richter-Menge J, Jeffries M (2011) The Arctic, in “State of the Climate in 2010”. *Bull Am Meteor Soc* 92(6):S143–S160
- Rudels B, Anderson LG, Jones EP (1996) Formation and evaluation of the surface mixed layer and halocline of the Arctic Ocean. *J Geophys Res* 101(C4):8807–8821
- Sandø AB, Nilsen JE, Gao Y, Lohmann K (2010) Importance of heat transport and local air-sea heat fluxes for Barents Sea climate variability. *J Geophys Res* 115(C07013). doi:[10.1029/2009JC005884](https://doi.org/10.1029/2009JC005884)
- Schauer U, Beszynniska-Möller A, Walczowski W, Fahrbach E, Piechura J, Hansen E (2008) Variation of measured heat flow through the Fram Strait between 1997 and 2006. In: Dickson B, Meincke J, Rhines P (eds) *Arctic-Subarctic ocean fluxes: defining the role of Nordic Seas in climate*, Chap 3. Springer, Berlin
- Schlichtholz P (2011) Influence of oceanic heat variability on sea ice anomalies in the Nordic Seas. *Geophys Res Lett* 38(L05705). doi:[10.1029/2010GL045894](https://doi.org/10.1029/2010GL045894)
- Semenov VA (2008) Influence of oceanic inflow to the Barents Sea on climate variability in the Arctic region. *Dokl Earth Sci* 418(1): 91–94
- Semenov VA, Park W, Latif M, (2009) Barents Sea inflow shutdown: a new mechanism for rapid climate changes. *Geophys Res Lett* 36(L14709). doi:[10.1029/2009GL038911](https://doi.org/10.1029/2009GL038911)
- Serreze MC, Barret AP, Stroeve JC, Kindig DN, Holland MM (2009) The emergence of surface-based Arctic amplification. *Cryosphere* 3:11–19
- Shimada K, Kamoshida T, Itoh M, Nishino S, Carmack E, McLaughlin F, Zimmerman S, Proshutinsky A (2006) Pacific Ocean inflow: influence on catastrophic reduction of sea ice cover in the Arctic Ocean. *Geophys Res Lett* 33:L08605. doi:[10.1029/2005GL025624](https://doi.org/10.1029/2005GL025624)
- Simonsen K, Haugan PM (1996) Heat budgets of the Arctic Mediterranean and sea surface heat flux parameterization for the Nordic Seas. *J Geophys Res* 101:6553–6576
- Skagseth Ø (2008) Recirculation of Atlantic Water in the western Barents Sea. *Geophys Res Lett* 35(L11606). doi:[10.1029/2008GL033785](https://doi.org/10.1029/2008GL033785)
- Skagseth Ø, Furevik T, Ingvaldsen R, Loeng H, Mork KA, Orvik KA, Ozhigin V (2008) Volume and heat transports to the Arctic Ocean via the Norwegian and Barents Seas. In: Dickson B, Meincke J, Rhines P (eds) *Arctic-subarctic ocean fluxes: defining the role of Nordic Seas in climate*, Chap 2. Springer, Berlin
- Smedsrud LH, Ingvaldsen R, Nilsen JE, Skagseth Ø (2010) Heat in the Barents Sea: transport, storage, and surface fluxes. *Ocean Sci* 6:219–234
- Sorteberg A, Kvingsedal B (2006) Atmospheric forcing in the Barents Sea winter sea ice extent. *J Clim* 19:4772–4784
- Spielhagen RF, Werner K, Aagaard Sørensen S, Zamelczyk K, Kandiano E, Budeus G, Husum K, Marchitto TM, Hald M (2011) Enhanced modern heat transfer to the arctic by warm Atlantic water. *Science* 331(6016):450–453. doi:[10.1126/science.1197397](https://doi.org/10.1126/science.1197397)
- Sterl A, Bintanja R, Brodeau L, Gleeson E, Koenigk T, Schmith T, Semmler T, Severijns C, Wyser K, Yang S (2012) A look at the ocean in the EC-Earth climate model. *Clim Dyn*. doi:[10.1007/s00382-011-1239-2](https://doi.org/10.1007/s00382-011-1239-2)
- Stroeve JC, Serreze MC, Holland MM, Kay JE, Malanik J, Barret AP (2012) The Arctic’s rapidly shrinking sea ice cover: a research synthesis. *Clim Change* 110:1005–1027. doi:[10.1007/s10584-011-0101-1](https://doi.org/10.1007/s10584-011-0101-1)
- Valcke S (2006) OASIS3 user guide (prism_2-5). PRISM support initiative report 3, p 64
- Van der Swaluw E, Drifhout SS, Hazeleger W (2007) Bjerknes compensation at high northern latitudes: the ocean forcing the atmosphere. *J Clim* 20:6023–6032
- Vavrus S, Holland M, Jahn A, Bailey D, Blazey B (2012) 21st-century Arctic climate change in CCSM4. *J Clim* 25:2696–2710. doi:[10.1175/JCLI-D-11-00220.1](https://doi.org/10.1175/JCLI-D-11-00220.1)
- Woodgate RA, Aagaard K (2005) Revising the Bering Strait freshwater flux into the Arctic Ocean. *Geophys Res Lett* 32(L02602). doi:[10.1029/2004GL021747](https://doi.org/10.1029/2004GL021747)
- Woodgate RA, Aagaard K, Weingartner TJ (2006) Interannual changes in the Bering Strait fluxes of volume, heat and freshwater between 1991 and 2004. *Geophys Res Lett* 33(L15609). doi:[10.1029/2006GL026931](https://doi.org/10.1029/2006GL026931)